Carbohydrate Polymers 224 (2019) 115188

Contents lists available at ScienceDirect

Carbohydrate Polymers

journal homepage: www.elsevier.com/locate/carbpol

Melt-processing of cellulose nanofibril/polylactide bionanocomposites via a sustainable polyethylene glycol-based carrier system

Jonathan Cailloux[a,*], Jean-Marie Raquez[b], Giada Lo Re[c], Orlando Santana[a], Leila Bonnaud[b], Philippe Dubois[b], Maria Lluïsa Maspoch[a]

[a] Centre Català del Plàstic, Universidad Politécnica de Cataluña Barcelona Tech (EEBE-UPC), C/Colom, 114, Terrassa 08222, Spain
[b] Laboratory of Polymeric and Composite Materials, Center of Innovation and Research in Materials & Polymers (CIRMAP), Materia Nova Research Center & University of Mons (UMONS), 23 Place du Parc, Mons B-7000, Belgium
[c] Department of Industrial and Materials Science, Chalmers University of Technology, Rännvägen 2, Gothenburg 412 96, Sweden

ARTICLE INFO

Keywords:
Polylactide
Cellulose nanofibrils
Polyethylene glycol
Sustainable process
Melt-processing

ABSTRACT

Considering the appealing need for an industrially viable approach, this works aims at demonstrating the rapid and easy melt processing of Polylactide (PLA) bio-composites reinforced with cellulose nanofibrils (CNF). For this purpose and against to their high propensity to self-aggregate on processing, an aqueous CNF-based suspension in the presence of polyethylene glycol (PEG) followed by a gentle drying way were performed to provide melt-processable CNF-based masterbatches. Morphological observations coupled with rheological analyses confirmed how the strategy of the PEG-based masterbatch approach facilitated the formation of a well-dispersed and strongly interacting CNF network within the polymeric matrix. At temperatures above T_g, thermo-mechanical characterization showed that the load-bearing capacity of the web-like CNF network was even more apparent and counteracted the PEG plasticizing effect. Thermogravimetric analysis evidenced that in the case of selective positioning at the PLA-PEG interface, CNF mitigated the negative impact of PEG addition on the PLA thermal stability. These results revealed the successfulness of our sustainable organic solvent-free approach to prepare melt-processable CNF masterbatches, which can be readily converted into conventional industrially scalable melt-processing techniques.

1. Introduction

Developing environmentally friendly thermoplastic composites reinforced with organic nanoscale fillers has become the focus of considerable research attention. In this context, cellulose reinforced polylactide (PLA) nanocomposites have attracted a great interest principally because of their entirely bio-based content and biodegradability (Azizi Samir, Alloin, & Dufresne, 2005; Ku, Wang, Pattarachaiyakoop, & Trada, 2011). Among all cellulose nanometer-sized fillers, there is a growing demand for using cellulose nanofibrils (CNF) as reinforcement material for PLA (Ling, Kaplan, & Buehler, 2018). Their high aspect ratio, associated with an outstanding mechanical stiffness and a low percolation threshold allowed to improve PLA crystallization capacity as well as rheological, mechanical and foaming properties at relatively low filler loadings (0.5–5 wt.%) (Cho, Park, Yun, & Jin, 2013; Ding, Kuboki, Wong, Park, & Sain, 2015; Safdari, Bagheriasl, Carreau, Heuzey, & Kamal, 2018).

Nevertheless, the difficulties for dispersing hydrophilic CNF into polymers restrict the full potential of CNF to solution casting methods (Kakroodi, Cheng, Sain, & Asiri, 2014; Kaushik, Singh, & Verma, 2010). Frequently, the dried and casted compound is used as a masterbatch and further melt processed to principally reinforced PLA matrix (Cho et al., 2013; Ding et al., 2015; A. N. Frone, Berlioz, Chailan, & Panaitescu, 2013; Jonoobi, Harun, Mathew, & Oksman, 2010; Kowalczyk, Piorkowska, Kulpinski, & Pracella, 2011; Safdari et al., 2018; T. Wang & Drzal, 2012; Yang, Li, Si, Cui, & Peng, 2019) among others (Sakakibara, Yano, & Tsujii, 2016; Sakakibara, Moriki, Yano, & Tsujii, 2017). Despite their efficiency, these preparation routes involve organic solvents and are time expensive, which makes them difficult to be scaled up. Therefore, melt-mixing is the key processing method suitable for large volume production. Although the manufacturing of cellulose nanocrystals (CNC)- or cellulose nanowiskers-reinforced PLA

* Corresponding author.
E-mail addresses: jonathan.cailloux@upc.edu (J. Cailloux), jean-marie.raquez@umons.ac.be (J.-M. Raquez), giadal@chalmers.se (G. Lo Re), orlando.santana@upc.edu (O. Santana), leila.bonnaud@materianova.be (L. Bonnaud), philippe.dubois@umons.ac.be (P. Dubois), maria.lluisa.maspoch@upc.edu (M.L. Maspoch).

https://doi.org/10.1016/j.carbpol.2019.115188
Received 24 May 2019; Received in revised form 7 August 2019; Accepted 8 August 2019
Available online 10 August 2019
0144-8617/

bionanocomposites using conventional industrially scalable melt-processing techniques has been widely reported (2007b, Ben Azouz, Ramires, Van den Fonteyne, El Kissi, & Dufresne, 2011; Bondeson & Oksman, 2007a; Martínez-Sanz, Lopez-Rubio, & Lagaron, 2012; Oksman, Mathew, Bondeson, & Kvien, 2006, 2016; Raquez et al., 2012), the extension of this method to CNF is rare (Kiziltas et al., 2016; Lo Re et al., 2018).

One of the main issues remain in the strong tendency of CNF to irreversible self-agglomeration as soon as they are dried due to their high aspect ratio, flexibility and large specific surface area rich in hydroxyl groups. Even using high shear extent, breaking up such irreversible agglomerates remains challenging, thus significantly restricting their filler reinforcing capacity based on the formation of a well-entangled percolated network within the matrix. Considering the need for an industrially viable approach, the wet-feeding method seems to be the approach of choice to provide solutions against CNF aggregation during drying. The development of a water-based wet-feeding method was reported to prepare CNF/polycaprolactone nanocomposites compatibilized with a latex form surfactant at 120 °C (Lo Re et al., 2018). Although results evidenced a significant enhancement of the mechanical properties resulting from an improved CNF dispersion, this preparation route is time consuming. An alternative technique consists in masterbatching CNF on the melted state. In this approach, polyhydroxybutyrate (PHB) was employed as carrier system for CNF before melt compounding with PLA (Kiziltas et al., 2016). Prior to diluting, the aqueous suspension of CNF was wet-fed into melted PHB at 170 °C. Even though interesting results were reported, the authors themselves recognized the hazardousness of the masterbatch processing, which limits the use of this technique in industrial processes.

This work aims to demonstrate the proof-of-the-concept regarding the potential of the masterbatch-assisted approach to obtain CNF-reinforced PLA bio-composites that can be processed on an industrial scale. Since CNF are obtained in the form of aqueous suspension, we implement a masterbatch preparation using a hydrosoluble polymer (such as polyethylene glycol, PEG). The solution casting mixture of PEG and CNC from water and the subsequent evaporation of the aqueous medium has already been proven to promote filler dispersion in melt processed nanocomposites (Ludueña et al., 2016; Zhang, Gao, Zou, & Wang, 2017).

In the present study, the challenge was to adjust and then to upscale the masterbatch procedure to prepare dried and concentrated melt-processable CNF dispersions which then can be directly incorporated into conventional industrially scalable melt-processing techniques. CNF obtained from the enzymatic process were selected because they exhibited higher molecular weight as well as crystallinity, with superior aspect ratio and they were more uniform as compared to CNF from acid pretreatment (Nie et al., 2018; Zimmermann, Pöhler, & Geiger, 2004). Composites with different PEG concentration (0, 10 and 20 wt.%) were prepared and the evolution of the filler dispersion was investigated through morphological observations and rheological analyses. The thermal, thermo-mechanical and mechanical properties are discussed and related to the degree of filler dispersion.

2. Materials and methods

2.1. Materials

A commercial PLA grade (Ingeo PLA 4032D, D-lactic content ≈ 2%, MFI (210 °C,2.16 kg) = 6.4 ± 0.3 g/10 min) was supplied by Natureworks LLC (Belgium). The weight-average molecular weight and the polydispersity index were approximately 190 kg.mol^{-1} and 1.9, respectively, as determined using size exclusion chromatography experiments in chloroform ($CHCl_3$). Polyethylene glycol (PEG) (MW ≈ 2000 g.mol^{-1}) was purchased from Alfa Aesar (Germany) and a sterically hindered phenolic primary antioxidant (Irganox 1010) was kindly supplied by BASF (Spain).

2.2. Extraction and preparation of enzymatic-CNF

An enzymatic pretreatment (Novozym 476) followed by eight passes through a microfluidizer (Microfluidics Inc., USA) were carried out on never-dried softwood pulp (supplied by Nordic Paper, Sweden) with 13.8 wt.% hemicellulose and 0.7 wt.% lignin, to prepare enzymatic-CNF (CNF), as reported elsewhere (Henriksson, Henriksson, Berglund, & Lindström, 2007). From the last pass through a microfluidizer, a viscous gel (≈1.5 wt.% dry content) of enzymatic-CNF was obtained. As shown in Fig. A.1. (c.f. Appendix A section), the diameter and length of the CNF were ~11.5 nm ± 4.0 nm and ~10 µm, respectively (Lo Re et al., 2018).

2.3. PLA/PEG/CNF bio-composite manufacturing

Two PEG-based masterbatches with a nominal content of dried CNF set at 20 and 33 wt.% were prepared by mixing PEG and the aqueous suspension of CNF in distilled water under continuous stirring for 3 h at room temperature (RT). The final mixtures were poured into glass Petri dishes, dried at 35 °C for 3 days and then ground into small flakes (< 5 mm diameter, to allow the feeding into the microcompounder). CNF alone were subjected to the same experimental protocol to obtain a reference sample.

The obtained flakes were melt compounded with PLA using a DSM Xplore Micro 15cc twin screw compounder (Netherlands) under a N_2 blanket to manufacture (nano)composite with a CNF nominal content of 5 wt.%. A screw speed of 100 rpm, a residence time of 2.5 min and a barrel temperature of 190 °C was used. Prior to processing, PLA was vacuum-dried at 60 °C overnight. Thermal degradations were counteracted by adding 0.5 wt.% of Irganox 1010. The nominal PLA/PEG/CNF ratios were 95/0/5; 85/10/5 and 75/20/5 and the samples were denoted as PLA/CNF, PLA/10PEG/CNF and PLA/20PEG/CNF, respectively. Disks (diameter: 25 mm; thickness: 1.5 mm) and rectangular bars (45 × 12 × 2 mm^3) were injected using a DSM Xplore Micro 5cc injection moulding machine (barrel temperature: 190 °C, mold temperature: 30 °C, pressure 8.5 bars). For comparison purposes, pure PLA and PLA/PEG blends (nominal ratios: 90/10 and 80/20 wt/wt) were manufactured following the same procedure.

2.4. Characterization techniques

2.4.1. Morphology observation

Optical microscopy (Nikon, Optiphot-Pol XTP-11) equipped with a cross-polarizer and scanning electron microscopy (SEM, JEOL, JSM −7001 F, Japan) were used to investigate the CNF dispersion within PLA. SEM observations were carried out on the cryogenically fractured surface of the injection moulded samples at 2 kV. Prior to observation, PLA and PEG were selectively extracted to assess the CNF distribution. Samples were immersed in a water-methanol solution (1:2 vol./vol.) containing 0.025 mol.L^{-1} of sodium hydroxide for 2 days at RT. Then, samples were sputter coated with a thin platinum-palladium layer.

2.4.2. Fourier transform infrared spectroscopy (FTIR)

The intramolecular interactions between PEG and CNF were investigated on the masterbatch flakes using FTIR. Absorption spectra were recorded on a Tensor 27 Standard System spectrometer (Bruker) in attenuated total reflectance mode in the 4000-600 cm^{-1} region with at a resolution of 4 cm^{-1} and 32 scans.

2.4.3. Differential scanning calorimetry (DSC)

DSC experiments were performed on a MDSC Q2000 instrument (TA Instrument) under a dry N_2 atmosphere. 5–6 mg of the samples were sealed in standard aluminium pans and subjected to a heating/cooling/heating procedure from -80 to 200 °C at a rate of 10 °C.min^{-1}. From the first and second heating scans, the degree of crystallinity, X_c, was calculated as follows:

$$X_c(\%) = \frac{\Delta H_m - \Delta H_{cc}}{\Delta H_m^0 * \varnothing_{PLA}} * 100 \quad (1)$$

Where ΔH_m is the melting enthalpy, ΔH_{cc} the cold crystallization enthalpy, φ_{PLA} the weight fraction of PLA and ΔH_m^0 the melting enthalpy for a 100% crystalline PLA (93.6 $J.g^{-1}$) (Hakim et al., 2017).

2.4.4. Rheological measurements

Dynamic rheological measurements were performed using an AR-G2 rheometer (TA Instruments) in parallel plate (25 mm) configuration at 180 °C under N_2 atmosphere. Small amplitude oscillatory experiments were carried out in the angular frequency range $1 < \omega < 623$ rad.s^{-1}at 3% strain (linear viscoelastic regime, L.V.R.). To ensure sufficient data in the terminal regime of CNF-reinforced samples, creep-recovery experiments were performed using fresh samples. The compliance data, J (t), were converted to dynamic measurements using the NLREG method (Honerkamp & Weese, 1993). The melt elasticity was measured using the elastic compliance, $J_r(t)$, through the steady-state elastic recovery compliance parameter, J_e^0 (Gabriel & Munstedt, 2002). Time sweep experiments confirmed stable rheological properties throughout analyses, with changes less than 10%.

2.4.5. Dynamic mechanical thermal analysis (DMTA)

DMTA was performed on rectangular samples using a Q800 DMTA equipment (TA Instruments). Specimens were tested in the dual cantilever bending mode at a frequency of 1 Hz, 0.02% of deformation (L.V.R) from -100 to 110 °C at a heating rate of 2 °C.min^{-1}. Data were averaged over three specimens for each formulation. Statistical differences between formulations were determined using a one-way ANOVA followed by a post hoc Tuckey's honesty significant difference (HSD) test. Differences were considered to be significant at $p < 0.05$.

2.4.6. Thermogravimetric analysis (TGA)

Thermal stability of the samples was investigated using a Q500 thermogravimetric analyser (TA Instruments) from 30 to 800 °C at a heating rate of 10 °C.min^{-1} under a dry N_2 gas flow rate of 60 mL/min.

3. Results and discussion

In Fig.1a, the cross-polarized light micrograph of PLA/CNF sample revealed the expected coarse suspension of large CNF aggregates, resulting from the high complexity in re-dispersing agglomerated CNF through melt processing (Lo Re & Sessini, 2018; Mathew, Oksman, & Sain, 2005; Peng, Gardner, & Han, 2012). The well-documented poor compatibility between both components was evidenced by clear vacancies at the polymer-aggregate interface (Fig. 1d). In contrast, a more homogeneous morphology was apparently obtained for both masterbatch-based samples. Polarized light microscopy evidenced a gradual reduction of the size of the CNF aggregates with the PEG content. The SEM micrographs of the cryo-fractured surfaces of the composites before the selective extraction of PLA and PEG (Fig. A.2) indicated a miscible PLA/PEG blend, without any evidence of phase separation for the low PEG content (PLA/10PEG/CNF). An initial phase separation can be seen in the composite holding 20 wt.% of PEG, with submicrometric domains, confirming the well-known partial miscibility between both polymers above 15 wt.% (Li, Zhang, Liang, & Wang, 2015; B. Wang, Hina, Zou, Zuo, & Yi, 2018).

The selective surface etching of PLA and PEG on the cryofractured surface allowed to assess CNF dispersion. While randomly oriented thin CNF were observed in PLA/10PEG/CNF (Fig. 1h), a network of highly entangled CNF with high aspect ratios was achieved with 20 wt.% PEG content (Fig. 1i). The SEM morphology after etching confirmed how the strategy of the PEG-based masterbatch assists not only in the dispersion of the CNF, but also improves the uniformity of the dispersion. Moreover, the evidence of the network formation for the high-level PEG content highlights the thermodynamic driving force of the nanofibrils towards the interface of the incipient immiscible PLA/PEG blend (Balazs, Emrick, & Russell, 2006). In polymer blends, nanoparticles have also shown to influence the phase-separation kinetics, coarsening their dynamics (Araki & Tanaka, 2006). In particular, a significant reduction in the domain size in phase-separated binary blends using clay sheets was evidenced as a result of their localization at the interface between the immiscible components (Si et al., 2006). Accordingly, this corroborated the formation of submicrometric domains of the PEG phase observed on the micrographs before the etching process (Fig. A.2), corresponding to the CNF distance after the polymer removal. Similarly, Scaffaro *et al.* stabilized the PLA/PEG morphology by the use of graphene oxide nanosheets, localized at the interphase (Scaffaro, Maio, Re, Parisi, & Busacca, 2018). CNC localization at the hydrophilic/hydrophobic polymer blend interphase was also reported by Lu et al. (Lu, Huang, Ge, Xie, & Wu, 2018).

As aforementioned, morphological observations suggested that PEG minimized CNF self-agglomeration through H-bonding during drying. At this regard, the intermolecular interactions between PEG and CNF were investigated on the masterbatch flakes using FTIR. Fig. A.3.a and A.3.b compare the spectra of both masterbatch flakes in the −OH and in the C−OC− stretching regions with that of CNF and PEG, respectively. While the maximum of the broad bands produced by the stretching of the −OH groups on the CNF surface shifted to slightly lower wavenumbers (3366 to 3342 cm^{-1}) in both PEG/CNF masterbatches, the energy needed to stretch the PEG ester bonds slightly increased (1096 to 1101 cm^{-1}) when adding CNF. These changes originated from the expected physical interactions between the ether oxygen groups of PEG and the hydroxyl groups on the cellulose surface via hydrogen bonding, as already reported elsewhere (Cheng et al., 2015; Kondo & Sawatari, 1994; Samir, Alloin, Sanchez, & Dufresne, 2004). This result was corroborated by suspension tests performed in THF. Fig. A.4 shows that the mixture of the CNF aqueous suspension and PEG was stable and well dispersed in THF, while the CNF aqueous suspension flocculated and then settled down in THF. Indeed, after adsorption on the CNF surface, PEG macromolecules spread into the organic solvent like polymer brushes, thus stabilizing the as-formed suspension against sedimentation (Phenrat et al., 2008).

Fig. 2 shows the DSC thermograms and Table 1 reports the main thermal parameters of all injection moulded samples. A more detailed analysis of the thermal parameters can be found in Table A.1. The first heating scans showed that PLA and PLA/CNF samples exhibited similar DSC traces. The slow PLA crystallization kinetics coupled with the high cooling rate during processing led to predominantly amorphous samples (Hakim et al., 2017). In PLA/PEG blends, the plasticizing effect of PEG on PLA shifted the PLA cold crystallization temperature, T_{cc}, to lower temperatures and enhanced the crystallization capacity of PLA (Li et al., 2015; Yu et al., 2015). Even though PLA melting temperature, T_m, remained almost constant, the drop in T_{cc} was lower when adding 20 wt.% PEG. This ascribed to the partial miscibility between both polymers, as evidenced in Fig. A.2. No significant differences in the DSC traces were observed between PLA/PEG/CNF and their PLA/PEG counterparts apart from a slight decrease in the achievable X_c. These data indicated that PEG chains exclusively interacted with PLA macromolecules, presumably due to a partial PEG desorption from the CNF surface during high shear twin-screw compounding.

In agreement with the first heating cycle, adding aggregated CNF did not improve the poor crystallization ability of PLA. From the melt, no crystallization peak was observed in the DSC cooling trace of PLA and PLA/CNF samples (Fig. 2b). The plasticizing effect of PEG can be observed as a well-defined crystallization transition for PLA in the DSC thermograms of both PLA/PEG blends, in which peak temperature, T_c, increased with the PEG content (Ahmed, Varshney, Auras, & Hwang, 2010; Li et al., 2015). The non-separation of T_c for PEG in PLA/10PEG is indicative of a miscible system. In contrast, when adding 20 wt.% PEG, the fractionated crystallization of PEG induced the apparition of two extra exothermic peaks, confirming that PEG is only partly miscible

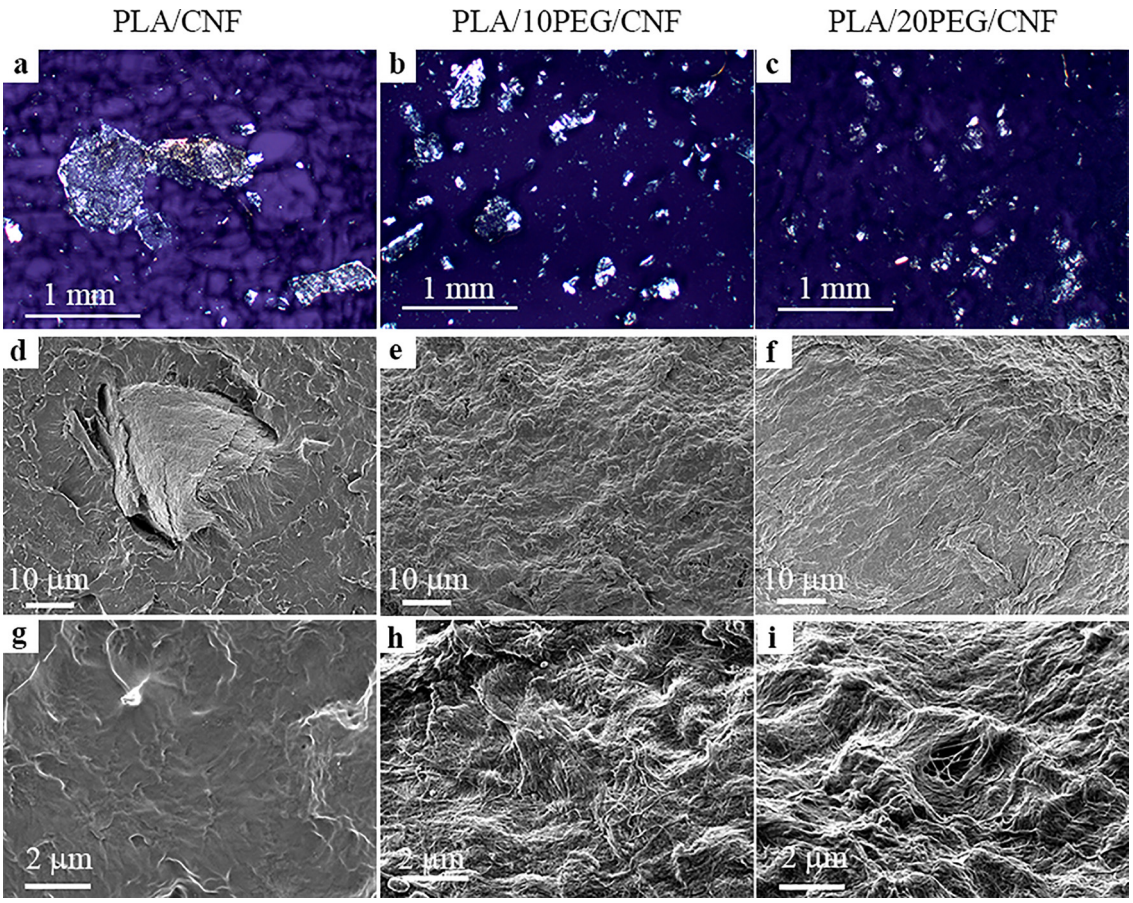

Fig. 1. Cross-polarized light micrographs (**a** to **c**) of all the CNF-reinforced samples. The regions exhibiting a strong birefringence show CNF aggregates. SEM micrographs (**d** to **i**) of the cryofractured surface after the selective surface etching of PLA and PEG.

within PLA when it content exceeds 10 wt.% (Li et al., 2015; B. Wang et al., 2018). In PLA/20PEG, the negative shift in T_c of PEG and the significant decrease in its achievable X_c as compared to pure PEG was ascribed to the physical confinement effect of PLA on the phase separated PEG domains (Ludueña et al., 2016).

On cooling from the melt, the well-established nucleating effect of cellulosic fillers on PLA was observed for the bio-composite holding 10 wt.% PEG content (Kose & Kondo, 2013). X_C value increased by 31% between PLA/10PEG and PLA/10PEG/CNF samples. This observation is in line with previous works and it was attributed to the large specific area of dispersed CNF that can promote PLA heterogeneous crystallization (Cho et al., 2013; Safdari et al., 2018; Suryanegara, Nakagaito, & Yano, 2009; Yang et al., 2019). Such effect was not clearly identified between samples with 20 wt.% of PEG, possibility due to the advanced plasticizing PEG effect, which dominated the crystallization process. Furthermore, the CNF network formation did not necessarily provide an optimistic morphology for enhancing PLA crystallization.

A rheological characterization was carried out in order to confirm the formation of a CNF network like structure within PLA and thus the efficiency of the PEG-based masterbatch approach. Fig. 3 shows the ω dependence of the complex viscosity, $|\eta^*|$, and the storage modulus, G', together with the Van-Gurp Palmen plots. PLA exhibited the typical pseudoplastic fluid behaviour. The continuously increasing tan (δ) behaviour as ω decreased was indicative of a predominant liquid-like behaviour (G" > G'), which increased upon PEG addition (Fig A.6). The expected gradual drop in η*, G' and J_e^0 values (Fig. 3) with the PEG

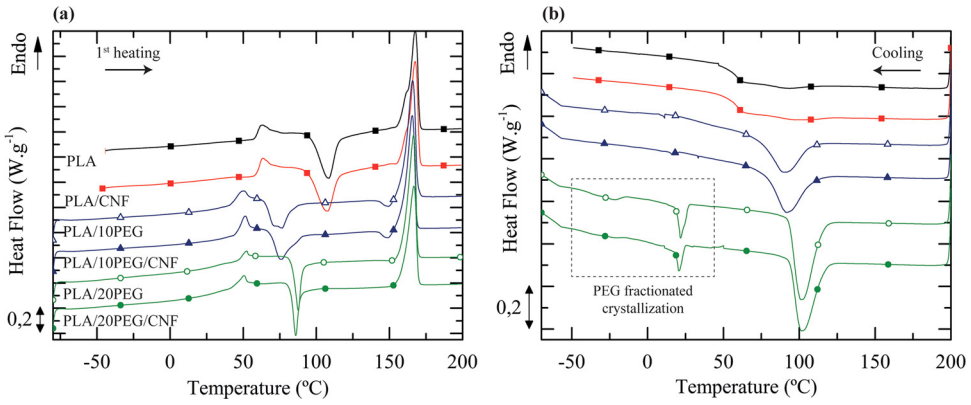

Fig. 2. a) First heating and **b)** cooling DSC scans at 10 °C.min^{-1}.

Table 1
Main thermal properties from the first heating and cooling DSC runs.

	PLA					PEG	
	1st heating run			Cooling run		Cooling run	
Sample	T_{cc} (°C)	T_m (°C)	X_c (%)	T_c (°C)	X_c [a] (%)	T_c (°C)	X_c [a] (%)
PEG	–	–	–	–	–	32.2	84
PLA	108.5	167.6	5	92.8	2	–	–
PLA/CNF	107.7	167.6	2	96.5	2	–	–
PLA/10PEG	75.7	165.9	22	86.5	26	–	–
PLA/10PEG/CNF	76.9	166	19	88.1	34	–	–
PLA/20PEG	16	166.9	32	103	52	21.7 / -21.6	24
PLA/20PEG/CNF	14	166.8	29	100.6	50	22.1 / -21.3	22

[a] X_c (%) = $\Delta H_c/(\Delta_m{}^o{}^*\varphi)^*100$, where φ is the weight fraction of the polymer considered and $\Delta H_m{}^0$ the melting enthalpy for a 100% crystalline PLA (93.6 J.g^{-1}) or PEG (208 J.g^{-1}), respectively (Hakim et al., 2017; Ludueña et al., 2016).

content was evidenced for plasticized PLA/PEG blends (Yu et al., 2015).

The addition of CNF alone decreased |η*|as compared to PLA over the whole experimental window (-13% in the zero-shear rate viscosity, η_0). Recall that the MW of the matrix and the degree of filler dispersion affect the rheological properties of nanocomposites. As compiled in Table A.2, MW averages agreed within 6% between PLA and PLA/CNF samples, suggesting that CNF did not promote PLA degradation. Accordingly, the lower viscosity could be primarily attributed to a possible disruption of the molecular network by the large CNF aggregates which lower the PLA viscous resistance. In the low ω region, CNF aggregates retarded the terminal PLA chains relaxation (higher G' and lower tan (δ) values than PLA), thus increasing the solid-like behaviour of the melt, as confirmed by the higher $J_e{}^0$ value (Fig. 3d).

Drastic changes in the rheological behaviour were observed when CNF were added to PLA via the PEG masterbatch approach. In fact, both PLA/PEG/CNF samples exhibited the characteristic rheological behaviour of structured fluids. The mechanical strengthening effect induced by CNF increased |η*| values over the whole experimental window as compared to their PLA/PEG counterparts. As ω decreased, the |η*| increase before reaching the Newtonian region is indicative of an apparent yield stress whose magnitude increased with the PEG content. Indeed, η_0 of PLA/20PEG/CNF exceeded that of PLA to almost one order of magnitude. The increasing time required for PLA/PEG/CNF bio-composites to flow gradually weakened the low-ω power-law dependence of G' before reaching the terminal regime and enhanced significantly the melt elasticity (Fig. 3d). All these changes indicated a gradual transition from liquid to solid-like behaviour due to the progressive formation of an interconnected CNF network (as shown in Fig. 1) wherein the fibre-fibre and/or fibre-polymer interactions significantly restricted the full relaxation of PLA chains (Ding et al., 2015; Safdari et al., 2018).

In the low ω region, these trends were reflected in the decreasing tan (δ) values with the PEG content (Fig A.5). PLA/20PEG/CNF exhibited tan (δ) values lower than 1 in the ω range of 0.005 - 0.2 rad.s^{-1}, indicating dominance of G' over G". These were supported by the Van Gurp-Palmen plots where the phase angle, δ = arctan(G"/G'), is plotted versus the complex modulus, G*. While a purely viscous behaviour is characterized by δ = 90°, a purely elastic melted material exhibits a δ value of 0°. PLA/20PEG/CNF displayed δ values lower than 45°, implying that the elastic component of the melt exceeded the viscous one. This transition is characteristic of solid-like composites and corroborated the formation of a strong space-spanning CNF network (Stokes & Telford, 2004). This result is consistent with the proposed possibility to control the morphology of partially miscible polymer blends using nanoparticles, as already discussed in the morphological analysis. Both the enthalpic and entropic interactions direct the spatial distribution of the nanofibrils and thereby control the macroscopic performance of the material, as the formation of the CNF interconnected network leading to liquid to solid behaviour transition (Balazs et al., 2006).

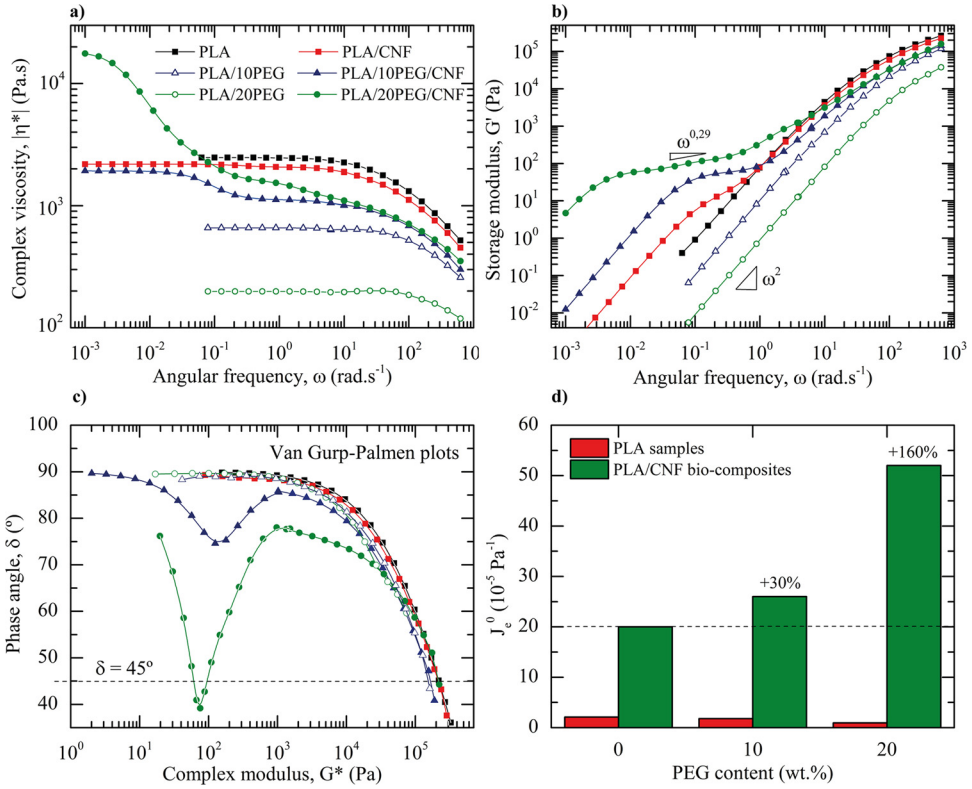

Fig. 3. ω dependence of the **a)** complex viscosity and **b)** storage modulus together with the **c)** Van Gurp-Palmen plots at 180 °C. **d)** Evolution of the steady-state elastic recovery compliance, $J_e{}^0$ for PLA samples and PLA/CNF bio-composites as a function of the PEG content.

Table 2
Summary of DMTA results *. The values in the parentheses are standard deviations.

	E' at -25 °C (GPa)	T_α (E")[a] (°C)	Damping factor[b]
PLA	4.1 (0.3)	54 (2)	22.7 (0.4)
PLA/CNF	4.21 (0.05)	55.9 (0.2)	24.2 (0.8)
PLA/10PEG	3.8 (0.2)	41.3 (0.4)	30 (1)
PLA/10PEG/CNF	4.3 (0.2)	41.4 (0.6)	26.5 (0.3)
PLA/20PEG	3.7 (0.5)	27 (1)	30 (1)
PLA/20PEG/CNF	3.9 (0.2)	29 (1)	27 (1)

*Fig. A.11 reported the Tukey's HSD analysis.
[a] T_α was determined as the point where E" reached a maximum.
[b] The damping factor corresponds to the area below the tan(δ) curve.

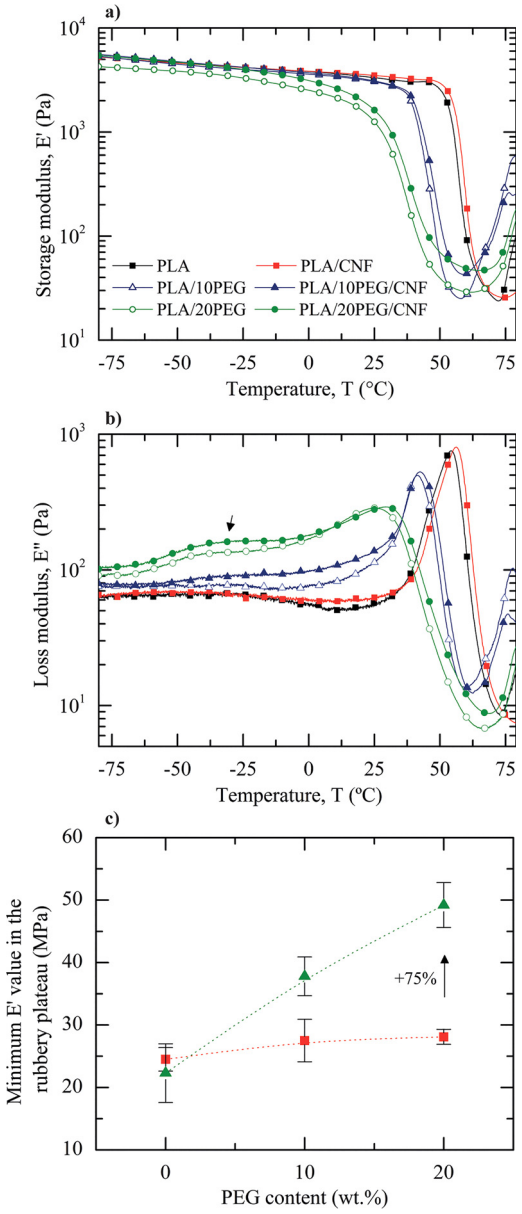

Fig. 4. a) and **b)** DMTA curves at 1 Hz. **c)** Evolution of the minimum E' value in the rubbery plateau for PLA samples (■) and PLA/CNF bio-composites (▲) as a function of the PEG content.

The mechanical properties of all the formulations were evaluated through uniaxial tensile experiments. Results are shown in Figs. A.7 – A.8 and Table A.3. Under tensile loading at RT, it is noteworthy that the CNF reinforcement efficiency in both bio-composites manufactured using the PEG masterbatch approach was limited due to the negative shift in T_g with the PEG content (Table 2), the partial miscibility exhibited by samples holding 20 wt.% of PEG and the well-established PEG migration issue from the bulk. Grafting of PEG on PLA via reactive extrusion could tackle these shortcomings (Hassouna et al., 2011) that will be the subject of a future study. In the present study, the efficiency of an improved CNF dispersion on the mechanical properties was better appraised through DMTA experiments. Fig. 4 displays the temperature variation of the storage modulus, E' and the loss modulus, E". E´ at -25 °C, the α-relaxation temperature, T_α, and the damping factor (DF, extent of chain mobility in the amorphous regions at T_g) are summarized in Table 2.

PLA exhibited the typical behaviour of amorphous polymers. During the controlled heating scan, sample stiffness remained fairly constant (≈ 4 GPa) over a wide range of temperature before experimenting a significant drop (between 50 and 70 °C) due to the glass-rubber transition (A. Frone, Berlioz, Chailan, Panaitescu, & Donescu, 2011). Upon further heating, E' raised around 75 °C due to the cold crystallization of PLA (Gupta, Simmons, Schueneman, Hylton, & Mintz, 2017; Safdari et al., 2018). In the temperature range where material softened, one characteristic peak was observed in both E" and tan (δ) traces (Fig. A.10) around 54 and 59 °C, respectively. This transition is related to the α-relaxation of the PLA chains and corresponds to the dynamic T_g of PLA (Safdari et al., 2018; Xiao et al., 2012). Based on the Tukey's HSD analysis (Fig A.11), results suggested that adding CNF alone did not statistically influence the PLA thermo-mechanical behaviour. The slight increase in the DF between PLA and PLA/CNF samples (Table 2) was ascribed to the small decrease in crystallinity upon CNF addition (Table 1, first heating scan) which enhanced the ability of the PLA backbones to dissipate the applied energy through segmental motions (A. Frone et al., 2011; Iwatake, Nogi, & Yano, 2008; Kowalczyk et al., 2011).

As expected, the elastic-like behaviour of PLA gradually declined with the PEG content in the glassy state (lower E' values at -25 °C for PLA/PEG blends than PLA in Table 2). The progressive decrease in T_g evidenced the plasticizing effect of an increasing PEG amount on PLA, which increased the damping extent at T_g and suppressed the load bearing contribution of the crystalline phase above T_g (Fig. 4c) (Tabi, Sajó, Szabó, Luyt, & Kovács, 2010). In PLA/20PEG blend, the partial miscibility between both polymers was further evidenced by the shoulder centred around −40 °C in the E" trace (indicated by an arrow in Fig. 4b), which can be assigned to the T_g of the immiscible PEG domains.

Interesting results were found when studying the storage modulus of CNF-reinforced PLA bio-composites manufactured using the PEG masterbatch approach. As reported in Fig. A.11, E' values in the glassy state between PLA and both PLA/PEG/CNF bio-composites were not statistically different. At temperatures above T_g, differences between the rubbery E' values were more noticeable (Fig. 4c). For instance, the minimum E' value in the rubbery plateau increased by 75% between PLA/20PEG and PLA/20PEG/CNF samples. Since PLA/PEG/CNF and PLA/PEG samples exhibited a similar X_c (Table 1), such increases cannot be attributed to a gradual reduction of the amorphous regions. PLA/PEG/CNF bio-composites are complex system where the plasticizing effect, attributed to PEG, competed with the reinforcing effect provided by CNF. As already evidenced in DSC, the previous physical adsorption of PEG chains on CNF did not restrain the PEG plasticizing effect on PLA. Accordingly, this behaviour can be explained by the creation of an increasingly stronger CNF network with increasing PEG content which resulted from strong interactions between nanofibrils by mechanical interlocking and contributed to the superior load-bearing capacity and decreased damping extend at T_g (Jonoobi et al., 2010; Saïd

Table 3
TGA results.

Sample nomenclature	$T_{5\%}$ (°C)	$T_{max,\ PLA}$ (°C)	$T_{max,\ PEG}$ (°C)
PLA	310.9	337.7	–
PEG	363.0	–	403.9
PLA/CNF	305.7	333.5	–
PLA/10PEG	288.7	330.1	386.2
PLA/10PEG/CNF	269.3	309.2	389.4
PLA/20PEG	255.8	298.1	388.7
PLA/20PEG/CNF	275.2	342.9	385.3

Azizi Samir et al., 2004). Regarding the PLA/20PEG/CNF sample, a statistically positive shift in T_α was evidenced as compared to the PLA/20PEG sample (Table 2 and Fig A.11). In this partially miscible system, this revealed that the presence of a web-like CNF network confined the molecular mobility of the PLA matrix (Safdari et al., 2018; Soeta et al., 2018).

The thermal stability of the samples was investigated using TGA and the first derivative of TGA (DTGA), as shown in Fig. A.12. Table 3 compiles the initial degradation temperature at 5% weight loss ($T_{5\%}$) and the maximum weight loss temperature of PLA ($T_{max,\ PLA}$) and PEG ($T_{max,\ PEG}$), respectively. The presence of CNF had no significant influence on the PLA thermal stability despite a slight decrease in the $T_{5\%}$. Both PLA/PEG blends experienced the expected two-stage weight loss. The first step reduction corresponds to the thermal decomposition of PLA while the second step, becoming more pronounced with increasing PEG content, corresponds to the decomposition of PEG. As compared to pure components, the thermal stability of PLA and PEG blends decreased, as already reported by (Ozdemir & Hacaloglu, 2017). $T_{5\%}$ of the blends gradually decreased as the PEG amount increased. Since PEG with a low MW was used, such decrease can be primarily ascribed to the reactions between the numerous −OH end groups of PEG and PLA ester functions (B. Wang et al., 2018). In PLA/20PEG/CNF sample, the localization of the CNF at the interface between PLA and the submicrometric PEG domains restricted the interactions between both components, thus mitigating the negative impact of PEG addition on the PLA thermal stability. Indeed, PLA/20PEG/CNF exhibited a slightly higher $T_{5\%}$ than PLA/20PEG sample and $T_{max\ PLA}$ shifted to higher temperatures as compared to PLA, indicating that the rate of thermal decomposition on the weight loss curve decreased. PLA/10PEG/CNF did not show such improvement due to the miscibility of PEG.

On the basis of all the previous results, Fig. 5 shows a scheme of the used strategy to manufacture PLA/PEG/CNF bionanocomposites. In the aqueous medium, the dispersed CNF interacted with the neighbouring PEG molecules through H-bonding and PEG molecules were wrapped around CNF. Increasing PEG content is likely to lead to an increase of the available macromolecular chains which can be physically adsorbed by the available specific area of CNF. After adsorption, this non-covalent polymeric "coating" acted as a physical steric hindrance agent between CNF during drying and prevented filler self-agglomeration. Through melt blending, partial PEG desorption from the CNF surface was presumed. However, the apparent quality of the CNF dispersion within PLA was improved, leading to the formation of a percolated CNF network when adding 20 wt.% PEG.

4. Conclusions

In this study, the difficulties of dispersing CNF into PLA through melt blending had been successfully minimized thanks to H-bonding

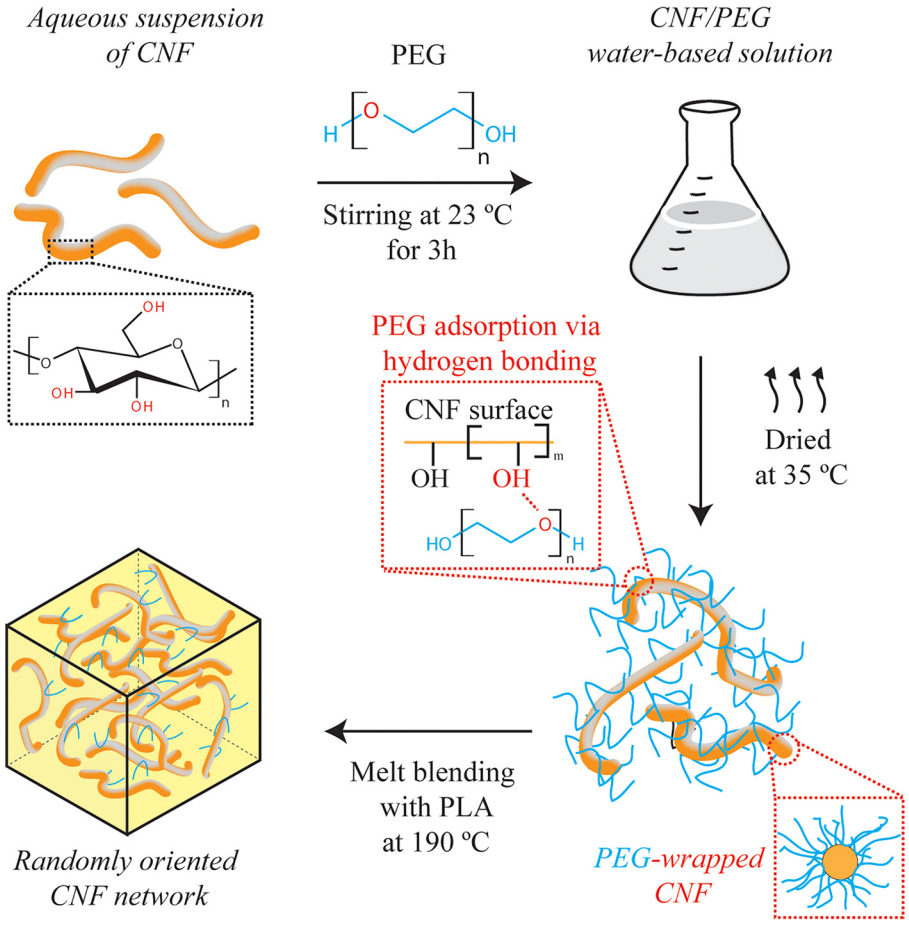

Fig. 5. Scheme of the manufacturing route of PLA/PEG/CNF bio-composites.

interactions between the hydrophilic polyethylene glycol (PEG) carrier system and the nanofillers. Results evidenced a progressive refinement of the CNF dispersion within PLA with the PEG content up to the formation of a well-entangled CNF network in the masterbatch-based composites holding 20 wt.% of PEG. Thermal analyses confirmed that dispersed CNF enhanced PLA crystallization when the plasticizing effect, attributed to PEG, did not dominate the crystallization process. The enhancement of the thermo-mechanical properties of the resulting PLA/PEG/CNF bio-composites demonstrated the load-bearing capacity of well-entangled CNF. Nevertheless, the well-known plasticizing effect of PEG decreased the glass transition temperature, lowering the reinforcement effect of CNF under tensile loading at room temperature. Thermogravimetric analysis evidenced that in the case of selective positioning at the PLA-PEG interface, CNF mitigated the negative impact of PEG addition on the PLA thermal stability. These promising results showed that the physical modification of CNF surface by PEG through a sustainable organic solvent-free process, lays the foundations for preparing dried and concentrated melt-processable CNF masterbatches which then can be adopted in conventional melt-processing methods at an industrial scale.

Acknowledgements

Authors thank the Spanish Ministry of Economy and Competitiveness for the Project MAT2016-80045-R (AEI/FEDER,UE). JMR as a FRS-FNRS research associate and LPCM is much indebted to both Wallonia and the European Commission “FSE and FEDER” for financial support in the frame of H2020-LCFM portofolio. G.L.R. acknowledges Knut and Alice Wallenberg Foundation KAW grant no. 2018.0451 Biokompositforskning and SSF grant no. GMT14/0036.

Appendix A. Supplementary data

Supplementary material related to this article can be found, in the online version, at doi:https://doi.org/10.1016/j.carbpol.2019.115188.

References

Ahmed, J., Varshney, S. K., Auras, R., & Hwang, S. W. (2010). Thermal and rheological properties of L-polylactide/polyethylene glycol/silicate nanocomposites films. *Journal of Food Science, 75*(8), N97–N108.

Araki, T., & Tanaka, H. (2006). Wetting-induced depletion interaction between particles in a phase-separating liquid mixture. *Physical Review E, 73*(6), 061506.

Azizi Samir, M. A. S., Alloin, F., & Dufresne, A. (2005). Review of recent research into cellulosic whiskers, their properties and their application in nanocomposite field. *Biomacromolecules, 6*(2), 612–626.

Balazs, A. C., Emrick, T., & Russell, T. P. (2006). Nanoparticle polymer composites: Where two small worlds meet. *Science, 314*(5802), 1107–1110.

Ben Azouz, K., Ramires, E. C., Van den Fonteyne, W., El Kissi, N., & Dufresne, A. (2011). Simple method for the melt extrusion of a cellulose nanocrystal reinforced hydrophobic polymer. *ACS Macro Letters, 1*(1), 236–240.

Bondeson, D., & Oksman, K. (2007a). Dispersion and characteristics of surfactant modified cellulose whiskers nanocomposites. *Composite Interfaces, 14*(7-9), 617–630.

Bondeson, D., & Oksman, K. (2007b). Polylactic acid/cellulose whisker nanocomposites modified by polyvinyl alcohol. *Composites Part A: Applied Science and Manufacturing, 38*(12), 2486–2492.

Cheng, D., Wen, Y., Wang, L., An, X., Zhu, X., & Ni, Y. (2015). Adsorption of polyethylene glycol (PEG) onto cellulose nano-crystals to improve its dispersity. *Carbohydrate Polymers, 123*, 157–163.

Cho, S. Y., Park, H. H., Yun, Y. S., & Jin, H.-J. (2013). Influence of cellulose nanofibers on the morphology and physical properties of poly (lactic acid) foaming by supercritical carbon dioxide. *Macromolecular Research, 21*(5), 529–533.

Ding, W., Kuboki, T., Wong, A., Park, C. B., & Sain, M. (2015). Rheology, thermal properties, and foaming behavior of high d-content polylactic acid/cellulose nanofiber composites. *RSC Advances, 5*(111), 91544–91557.

Frone, A., Berlioz, S., Chailan, J. F., Panaitescu, D., & Donescu, D. (2011). Cellulose fiber-reinforced polylactic acid. *Polymer Composites, 32*(6), 976–985.

Frone, A. N., Berlioz, S., Chailan, J.-F., & Panaitescu, D. M. (2013). Morphology and thermal properties of PLA–cellulose nanofibers composites. *Carbohydrate Polymers, 91*(1), 377–384.

Gabriel, C., & Munstedt, H. (2002). Influence of long-chain branches in polyethylenes on linear viscoelastic flow properties in shear. *Rheologica Acta, 41*(3), 232–244.

Gupta, A., Simmons, W., Schueneman, G. T., Hylton, D., & Mintz, E. A. (2017). Rheological and thermo-mechanical properties of poly (lactic acid)/lignin-coated cellulose nanocrystal composites. *ACS Sustainable Chemistry & Engineering, 5*(2), 1711–1720.

Hakim, R., Cailloux, J., Santana, O., Bou, J., Sánchez-Soto, M., Odent, J., & Maspoch, M. L. (2017). PLA/SiO2 composites: Influence of the filler modifications on the morphology, crystallization behavior, and mechanical properties. *Journal of Applied Polymer Science, 134*(40), 45367–45372.

Hassouna, F., Raquez, J.-M., Addiego, F., Dubois, P., Toniazzo, V., & Ruch, D. (2011). New approach on the development of plasticized polylactide (PLA): Grafting of poly (ethylene glycol)(PEG) via reactive extrusion. *European Polymer Journal, 47*(11), 2134–2144.

Henriksson, M., Henriksson, G., Berglund, L., & Lindström, T. (2007). An environmentally friendly method for enzyme-assisted preparation of microfibrillated cellulose (MFC) nanofibers. *European Polymer Journal, 43*(8), 3434–3441.

Honerkamp, J., & Weese, J. (1993). A nonlinear regularization method for the calculation of relaxation spectra. *Rheologica Acta, 32*(1), 65–73.

Iwatake, A., Nogi, M., & Yano, H. (2008). Cellulose nanofiber-reinforced polylactic acid. *Composites Science and Technology, 68*(9), 2103–2106.

Jonoobi, M., Harun, J., Mathew, A. P., & Oksman, K. (2010). Mechanical properties of cellulose nanofiber (CNF) reinforced polylactic acid (PLA) prepared by twin screw extrusion. *Composites Science and Technology, 70*(12), 1742–1747.

Kakroodi, A. R., Cheng, S., Sain, M., & Asiri, A. (2014). Mechanical, thermal, and morphological properties of nanocomposites based on polyvinyl alcohol and cellulose nanofiber from Aloe vera rind. *Journal of Nanomaterials, 2014*, 139.

Kaushik, A., Singh, M., & Verma, G. (2010). Green nanocomposites based on thermoplastic starch and steam exploded cellulose nanofibrils from wheat straw. *Carbohydrate Polymers, 82*(2), 337–345.

Kiziltas, A., Nazari, B., Kiziltas, E. E., Gardner, D. J., Han, Y., & Rushing, T. S. (2016). Method to reinforce polylactic acid with cellulose nanofibers via a polyhydroxybutyrate carrier system. *Carbohydrate Polymers, 140*, 393–399.

Kondo, T., & Sawatari, C. (1994). Intermolecular hydrogen bonding in cellulose/poly (ethylene oxide) blends: Thermodynamic examination using 2, 3-di-O-and 6-O-methylcelluloses as cellulose model compounds. *Polymer, 35*(20), 4423–4428.

Kose, R., & Kondo, T. (2013). Size effects of cellulose nanofibers for enhancing the crystallization of poly (lactic acid). *Journal of Applied Polymer Science, 128*(2), 1200–1205.

Kowalczyk, M., Piorkowska, E., Kulpinski, P., & Pracella, M. (2011). Mechanical and thermal properties of PLA composites with cellulose nanofibers and standard size fibers. *Composites Part A: Applied Science and Manufacturing, 42*(10), 1509–1514.

Ku, H., Wang, H., Pattarachaiyakoop, N., & Trada, M. (2011). A review on the tensile properties of natural fiber reinforced polymer composites. *Composites Part B: Engineering, 42*(4), 856–873.

Li, F. J., Zhang, S. D., Liang, J. Z., & Wang, J. Z. (2015). Effect of polyethylene glycol on the crystallization and impact properties of polylactide-based blends. *Polymers for Advanced Technologies, 26*(5), 465–475.

Ling, S., Kaplan, D. L., & Buehler, M. J. (2018). Nanofibrils in nature and materials engineering. *Nature Reviews Materials, 3*, 18016.

Lo Re, G., Engstrom, J., Wu, Q., Malmström, E., Gedde, U. W., Olsson, R. T., ... Berglund, L. A. (2018). Improved cellulose nanofibril dispersion in melt-processed polycaprolactone nanocomposites by a latex-mediated interphase and wet feeding as LDPE alternative. *ACS Applied Nano Materials, 1*(6), 2669–2677.

Lo Re, G., & Sessini, V. (2018). Wet feeding approach for cellulosic materials/PCL biocomposites. In A. Ayoub, & L. Lucia (Eds.). *Biomass extrusion and reaction technologies: Principles to practices and future potential* (pp. 209–226). .

Lu, Y., Huang, J., Ge, L., Xie, W., & Wu, D. (2018). Selective localization of cellulose nanocrystals in the biodegradable poly (vinyl alcohol)/poly (ε-caprolactone) blend composites prepared by Pickering emulsions. *Polymer, 156*, 136–147.

Ludueña, L. N., Fortunati, E., Morán, J. I., Alvarez, V. A., Cyras, V. P., Puglia, D., ... Pracella, M. (2016). Preparation and characterization of polybutylene-succinate/poly (ethylene-glycol)/cellulose nanocrystals ternary composites. *Journal of Applied Polymer Science, 133*(15), 43302–43311.

Martínez-Sanz, M., Lopez-Rubio, A., & Lagaron, J. M. (2012). Optimization of the dispersion of unmodified bacterial cellulose nanowhiskers into polylactide via melt compounding to significantly enhance barrier and mechanical properties. *Biomacromolecules, 13*(11), 3887–3899.

Mathew, A. P., Oksman, K., & Sain, M. (2005). Mechanical properties of biodegradable composites from poly lactic acid (PLA) and microcrystalline cellulose (MCC). *Journal of Applied Polymer Science, 97*(5), 2014–2025.

Nie, S., Zhang, K., Lin, X., Zhang, C., Yan, D., Liang, H., ... Wang, S. (2018). Enzymatic pretreatment for the improvement of dispersion and film properties of cellulose nanofibrils. *Carbohydrate Polymers, 181*, 1136–1142.

Oksman, K., Aitomäki, Y., Mathew, A. P., Siqueira, G., Zhou, Q., Butylina, S., ... Hooshmand, S. (2016). Review of the recent developments in cellulose nanocomposite processing. *Composites Part A: Applied Science and Manufacturing, 83*, 2–18.

Oksman, K., Mathew, A. P., Bondeson, D., & Kvien, I. (2006). Manufacturing process of cellulose whiskers/polylactic acid nanocomposites. *Composites Science and Technology, 66*(15), 2776–2784.

Ozdemir, E., & Hacaloglu, J. (2017). Characterizations of PLA-PEG blends involving organically modified montmorillonite. *Journal of Analytical and Applied Pyrolysis, 127*, 343–349.

Peng, Y., Gardner, D. J., & Han, Y. (2012). Drying cellulose nanofibrils: In search of a suitable method. *Cellulose, 19*(1), 91–102.

Phenrat, T., Saleh, N., Sirk, K., Kim, H.-J., Tilton, R. D., & Lowry, G. V. (2008). Stabilization of aqueous nanoscale zerovalent iron dispersions by anionic polyelectrolytes: adsorbed anionic polyelectrolyte layer properties and their effect on aggregation and sedimentation. *Journal of Nanoparticle Research, 10*(5), 795–814.

Raquez, J.-M., Murena, Y., Goffin, A.-L., Habibi, Y., Ruelle, B., DeBuyl, F., ... Dubois, P.

(2012). Surface-modification of cellulose nanowhiskers and their use as nanoreinforcers into polylactide: A sustainably-integrated approach. *Composites Science and Technology, 72*(5), 544–549.
Safdari, F., Bagheriasl, D., Carreau, P. J., Heuzey, M. C., & Kamal, M. R. (2018). Rheological, mechanical, and thermal properties of polylactide/cellulose nanofiber biocomposites. *Polymer Composites, 39*(5), 1752–1762.
Saïd Azizi Samir, M. A., Alloin, F., Paillet, M., & Dufresne, A. (2004). Tangling effect in fibrillated cellulose reinforced nanocomposites. *Macromolecules, 37*(11), 4313–4316.
Sakakibara, K., Moriki, Y., Yano, H., & Tsujii, Y. (2017). Strategy for the improvement of the mechanical properties of cellulose nanofiber-reinforced high-density polyethylene nanocomposites using diblock copolymer dispersants. *ACS Applied Materials & Interfaces, 9*(50), 44079–44087.
Sakakibara, K., Yano, H., & Tsujii, Y. (2016). Surface engineering of cellulose nanofiber by adsorption of diblock copolymer dispersant for green nanocomposite materials. *ACS Applied Materials & Interfaces, 8*(37), 24893–24900.
Samir, M. A. S. A., Alloin, F., Sanchez, J.-Y., & Dufresne, A. (2004). Cellulose nanocrystals reinforced poly (oxyethylene). *Polymer, 45*(12), 4149–4157.
Scaffaro, R., Maio, A., Re, G. L., Parisi, A., & Busacca, A. (2018). Advanced piezoresistive sensor achieved by amphiphilic nanointerfaces of graphene oxide and biodegradable polymer blends. *Composites Science and Technology, 156*, 166–176.
Si, M., Araki, T., Ade, H., Kilcoyne, A., Fisher, R., Sokolov, J. C., ... Rafailovich, M. H. (2006). Compatibilizing bulk polymer blends by using organoclays. *Macromolecules, 39*(14), 4793–4801.
Soeta, H., Lo Re, G., Masuda, A., Fujisawa, S., Saito, T., Berglund, L. A., ... Isogai, A. (2018). Tailoring nanocellulose–Cellulose triacetate interfaces by varying the surface grafting density of poly (ethylene glycol). *ACS Omega, 3*(9), 11883–11889.
Stokes, J., & Telford, J. (2004). Measuring the yield behaviour of structured fluids. *Journal of Non-Newtonian Fluid Mechanics, 124*(1-3), 137–146.
Suryanegara, L., Nakagaito, A. N., & Yano, H. (2009). The effect of crystallization of PLA on the thermal and mechanical properties of microfibrillated cellulose-reinforced PLA composites. *Composites Science and Technology, 69*(7-8), 1187–1192.
Tabi, T., Sajó, I., Szabó, F., Luyt, A., & Kovács, J. (2010). Crystalline structure of annealed polylactic acid and its relation to processing. *Express Polymer Letters, 4*(10), 659–668.
Wang, B., Hina, K., Zou, H., Zuo, D., & Yi, C. (2018). Thermal, crystallization, mechanical and decomposition properties of poly (lactic acid) plasticized with poly (ethylene glycol). *Journal of Vinyl and Additive Technology, 24*, E154–E163.
Wang, T., & Drzal, L. T. (2012). Cellulose-nanofiber-reinforced poly (lactic acid) composites prepared by a water-based approach. *ACS Applied Materials & Interfaces, 4*(10), 5079–5085.
Xiao, L., Mai, Y., He, F., Yu, L., Zhang, L., Tang, H., ... Yang, G. (2012). Bio-based green composites with high performance from poly (lactic acid) and surface-modified microcrystalline cellulose. *Journal of Materials Chemistry, 22*(31), 15732–15739.
Yang, Z., Li, X., Si, J., Cui, Z., & Peng, K. (2019). Morphological, mechanical and thermal properties of poly (lactic acid)(PLA)/cellulose nanofibrils (CNF) composites nanofiber for tissue engineering. *Journal of Wuhan University of Technology-Mater. Sci. Ed. 34*(1), 207–215.
Yu, Y., Cheng, Y., Ren, J., Cao, E., Fu, X., & Guo, W. (2015). Plasticizing effect of poly (ethylene glycol) s with different molecular weights in poly (lactic acid)/starch blends. *Journal of Applied Polymer Science, 132*(16), 41808–41817.
Zhang, P., Gao, D., Zou, P., & Wang, B. (2017). Preparation and thermomechanical properties of nanocrystalline cellulose reinforced poly (lactic acid) nanocomposites. *Journal of Applied Polymer Science, 134*(14), 44683–44692.
Zimmermann, T., Pöhler, E., & Geiger, T. (2004). Cellulose fibrils for polymer reinforcement. *Advanced Engineering Materials, 6*(9), 754–761.